frontiers | Frontiers in Nuclear Engineering

TYPE Original Research
PUBLISHED 20 June 2023
DOI 10.3389/fnuen.2023.1214727

OPEN ACCESS

EDITED BY
David Cheneler,
Lancaster University, United Kingdom

REVIEWED BY
Adam Burak,
University of Michigan, United States
David Abrecht,
Oak Ridge National Laboratory (DOE), United States

*CORRESPONDENCE
Samuel A. Walker,
Samuel.walker@inl.gov

RECEIVED 30 April 2023
ACCEPTED 06 June 2023
PUBLISHED 20 June 2023

CITATION
Walker SA, Tano ME, Abou-Jaoude A and Calvin O (2023), Depletion-driven thermochemistry of molten salt reactors: review, method, and analysis.
Front. Nucl. Eng. 2:1214727.
doi: 10.3389/fnuen.2023.1214727

Depletion-driven thermochemistry of molten salt reactors: review, method, and analysis

Samuel A. Walker*, Mauricio E. Tano, Abdalla Abou-Jaoude and Olin Calvin

Idaho National Laboratory, Idaho Falls, ID, United States

Molten salt reactors (MSRs) are innovative advanced nuclear reactors that utilize nuclear fuel by dissolving it in a high-temperature liquid salt. This unique feature differentiates MSRs from other types of reactors and allows for enhanced safety and economic performance. The liquid fuel also entails several multiphysics effects that can complicate reactor design and operation. One primary effect termed here as depletion-driven thermochemistry is a driving force in altering the multiphysics behavior of the reactor. Essentially, depletion-driven thermochemistry is the effect that fuel depletion has on changing the chemical redox potential of the fuel salt over time. As the fuel is consumed, the redox potential shifts toward a more oxidizing state. Without active control, the changing chemistry due to depletion increases corrosion thereby limiting reactor component lifetimes. Additionally, the changing redox potential of the fuel salt alters the vapor pressures of chemical species dissolved in the fuel salt. Changing vapor pressures of species in the fuel salt is an important parameter to understand when off-gassing volatile species during normal reactor operation, and for source term characterization during accident scenario transients. The present work represents a fundamental step toward modeling and coupling the driving physics (i.e., neutronics and chemistry) involved in altering the redox potential in an MSR. Here, the neutronic code Griffin models the depletion of the fuel-salt system, while the chemical equilibrium code Thermochimica calculates the thermochemical state of the isotopic inventory, using the Molten Salt Thermodynamic Database - Thermochemical (MSTDB-TC). These two codes are tightly coupled to predict the impact of fuel depletion in altering the chemistry in MSR systems. Redox potential control methods are discussed and can be modeled using this multiphysics approach. The vapor pressures of chemical species that could be extracted to an off-gas system, as determined by the reactor's thermochemical state, are examined. The neutronics-chemistry coupling developed in this work is expected to have potential application for analyzing corrosion, source term evolution, and material safeguards in MSR systems. Lastly, suggestions for areas of further improvements of the models to expand these capabilities by incorporating other coupled physics effects is provided.

KEYWORDS

molten salt reactors (MSR), depletion driven thermochemistry, source term, redox potential, multiphysics coupling

1 Introduction

Molten salt reactors (MSRs) utilize nuclear fuel dissolved in molten salt that can be pumped around a primary loop or kept roughly stagnant in pipes placed within the core. Due to the nature of their liquid fuel design, MSRs are considered to have the lowest technology readiness level (TRL) of all Generation IV nuclear reactors, as they are essentially a nuclear/chemical reactor hybrid (Gougar et al., 2015).

To increase the TRL of MSRs, private and public research focused on this cutting-edge reactor type has increased in recent years. Many MSR advocates strongly believe that investing in this unique advanced reactor type will reap distinct benefits in comparison to more traditional advanced reactor designs based on solid nuclear fuel. Thanks to the liquid nuclear fuel, MSRs open the possibility of designing ingenious and enhanced passive safety, online reprocessing schemes for fuel-cycle flexibility, and alternative economic uses for nuclear power including industrial heat and isotope production (Mignacca and Locatelli, 2020). For these reasons, MSR development is an attractive option for advanced nuclear reactor deployment. However, these reactor concepts are not without their drawbacks---mainly the low TRL that MSRs must overcome, and the utilization of an engineering methodology not traditionally seen in the nuclear engineering field for other reactors. Whereas solid-fueled reactors allow researchers and engineers to organize reactor analyses and design more easily into distinct physics (e.g., neutronics, thermal hydraulics, coolant chemistry, *etc.*), the physics of liquid-fueled reactors are inherently tightly coupled. This ultimately requires that MSRs are analyzed and designed in a manner that accounts for their multiphysics behavior (Abou-Jaoude et al., 2021).

One primary multiphysics phenomenon that drives the long-term behavior of MSRs during their operational lifetime is depletion-driven thermochemistry (Walker et al., 2023). Simply defined, depletion-driven thermochemistry is the process where the thermochemical equilibrium of the MSR fuel salt changes over time as the dissolved nuclear fuel is consumed and fission products (FPs) are generated via depletion. The new chemical species formed by FPs in the liquid salt may precipitate or volatilize into non-soluble species and hence, separate from the fuel salt and change the depletion evolution of the reactor. Additionally, this multiphysics process has several ramifications including corrosion, the behavior of volatile nuclide species, and the integral behavior of the reactor during normal operation and accident scenario transients (Walker and Ji, 2021a). Therefore, a multiphysics modeling and simulation approach, which couples fuel depletion and equilibrium thermochemistry, is an essential first step in modeling and designing MSR systems.

The work presented here represents a critical initial step toward building such modeling and simulation tools and identifying the experimental and thermochemical data limitations that remain. A new depletion-driven thermochemistry analysis capability was developed and implemented by coupling the U.S. Department of Energy's (DOE) Nuclear Energy Advanced Modeling and Simulation (NEAMS) neutronics code Griffin (Lee et al., 2021) with the open-source Gibbs Energy Minimizer (GEM) Thermochimica (Poschmann et al., 2021). Here, Griffin performs a multi-region depletion calculation of the fuel salt with gaseous nuclide removal and Thermochimica performs a thermochemical equilibrium calculation of the fuel-salt composition using the Molten Salt Thermodynamic Database–Thermochemical (MSTDB-TC) (Ard et al., 2022).

The following sections delve into the specifics of this multiphysics modeling and simulation work elucidating depletion-driven thermochemistry in MSR systems. Section 2 further identifies, defines, and describes in detail the multiphysics effect named here as "depletion-driven thermochemistry". Additionally, the state of the art of research on this topic is presented by way of a literature review, and the objective of this work in relation to the existing body of previous work is presented. The computational methodology and multiphysics coupling scheme of depletion and thermochemistry used in this work are detailed in Section 3.

In Section 4, the resulting multiphysics depletion-driven thermochemistry modeling capability is then applied to simulate the changing chemistry of both fluoride and chloride fuel-salt systems as depletion occurs. Additionally, chemical species and their associated vapor pressures in the fuel salt are identified, the availability of thermochemical data is discussed, and active chemistry control of fuel salts is simulated using this approach. Lastly, conclusions and key findings are reported and discussed in Section 5, along with a discussion of the future work necessary to more accurately model this multiphysics problem.

2 Review of depletion-driven thermochemistry

This section primarily introduces the multiphysics phenomenon that this work seeks to model via multiphysics simulations. The importance of depletion-driven thermochemistry in MSR systems is identified and its effect during the Molten Salt Reactor Experiment (MSRE) is described. The existing state of the art research capability is reviewed, and the objective of this work is discussed.

2.1 Defining depletion-driven thermochemistry

One of the largest remaining challenges in predicting MSR multiphysics behavior lies in understanding how the chemistry of fuel-bearing molten salts will change over the reactor lifetime as the MSR fuel salt undergoes depletion and how, in turn, chemical changes in the molten salt will affect the isotopic evolution of the reactor. This multiphysics coupling is coined by this work as "depletion-driven thermochemistry". It is defined as the neutronic-driven changes in the fuel salt chemistry over time due to the process of depletion. Here, thermochemistry refers to the chemical compounds and chemical state of the molten salt ionic liquid, while depletion refers to the process of fission, decay, and neutron capture that depletes the fissionable material and creates an extensive inventory of fission and activation products in the fuel salt.

2.1.1 Definition of the redox potential in relation to the fluorine or chlorine potential

The chemical behavior of molten salts is largely dependent on the redox potential of the fuel salt. The baseline potential for measuring the redox potential is conveniently stated in reference to the chemical potential of the base ion of the ionic salt (i.e., fluorine or chlorine chemical potential) as seen in Eq 1 (Olander, 2002). Here, R is the ideal gas constant in units of [J/(mol - °K)], T is the temperature of salt in °K, and p_{F_2} is the unitless partial pressure of fluorine gas (i.e., $F_{2(g)}$) in the molten salt, so the units of $\Delta\bar{G}_{F_2}$ are most commonly [J/mol] or [kcal/mol].

$$\Delta\bar{G}_{F_2} \equiv RT\,ln\,p_{F_2} \tag{1}$$

Additionally, the fluorine chemical potential can be related to the electrochemical potential of the molten salt via Eq 2 (Kelleher, 2013).

$$\Delta\bar{G}_{F_2} \equiv RT\,ln\,p_{F_2} = -nFE \tag{2}$$

Here, F = 96,485 [C/mol] is the Faraday constant representing the amount of charge per mol of electrons and n is the number of electrons transferred in the reaction where the standard state reaction is given as Eq 3 (Baes, Jr, 1965). The reference potential for the standard state half-cell reaction is set at 0 [V] as shown in Eq 3.

$$F_{2(g)} + 2e^- \leftrightarrow 2F^-,\ E^O = 0\ [V] \tag{3}$$

Essentially the fluorine chemical potential is a measurement of how strongly the fluorine in a system can oxidize/dissolve other elements in the system. In the remainder of this article, the electrochemical redox potential and the fluorine or chlorine chemical potential of the fuel salt will be used interchangeably with the understanding that the potential we refer to is linked to the base ion in the modeled salt system.

2.1.2 Importance of depletion-driven thermochemistry in molten salt reactors

The fluorine or chlorine potential of fluoride and chloride salts, respectively, is heavily influenced by the chemical composition of cations present which make up the ionic molten salt (Baes, Jr, 1965). During normal reactor operations, the chemical composition of the fuel salt will gradually change as the fuel salt undergoes nuclear fission, causing the fissionable heavy metals to be replaced with soluble or insoluble FPs. Additionally, non-fission transmutation of the fuel salt through capture reactions and radioactive decay will also occur altering the concentrations of actinides (e.g., neptunium, plutonium, *etc.*) as well as FPs in the fuel salt. The fuel salt chemical composition can also be altered by chemical species extracted from the fuel salt via off-gassing of volatile species or by additions of metallic nuclides to the fuel salt in the form of soluble species that are then dissolved in the fuel salt.

These changes in chemical composition due to depletion directly alter the fuel salt's redox potential, which in turn determines how the fuel and FPs behave in solution, as well as how structural materials interact with the salt via corrosion mechanisms. Therefore, depletion-driven thermochemistry is a critical driving force in determining reactor behavior during normal operation and accident scenarios. This includes long-term corrosion effects on key reactor components and how radionuclide source terms (dictated by nuclide vapor pressures) in the molten salt evolve over reactor lifetimes. Ultimately, this multiphysics effect is an essential consideration for future MSR reactor design, licensing, and operation.

TABLE 1 Calculated Electrode Potential in LiF-0.33BeF_2 (1,000 K)–Reformatted from (Baes, Jr, 1965).

Half Cell Reactions	E^O (1,000 [°K]), [V]
$Li^+ + e^- \Leftrightarrow Li_{(s)}$	−5.412
$La^{3+} + 3e^- \Leftrightarrow La_{(s)}$	−5.081
$Ce^{3+} + 3e^- \Leftrightarrow Ce_{(s)}$	−5.011
$Sm^{3+} + 3e^- \Leftrightarrow Sm_{(s)}$	−4.881
$Th^{4+} + 4e^- \Leftrightarrow Th_{(s)}$	−4.601
$Be^{2+} + 2e^- \Leftrightarrow Be_{(s)}$	−4.592
$U^{3+} + 3e^- \Leftrightarrow U_{(s)}$	−4.281
$U^{4+} + 4e^- \Leftrightarrow U_{(s)}$	−4.190
$Zr^{4+} + e^- \Leftrightarrow Zr_{(s)}$	−4.187
$U^{4+} + e^- \Leftrightarrow U^{3+}$	−3.915
$Cr^{2+} + 2e^- \Leftrightarrow Cr_{(s)}$	−3.261
$Fe^{2+} + 2e^- \Leftrightarrow Fe_{(s)}$	−2.882
$HF_{(g)} + e^- \Leftrightarrow F^- + ½H_{2\ (g)}$	−2.871
$Ni^{2+} + 2e^- \Leftrightarrow Ni_{(s)}$	−2.398
$½F_2(g) + e \Leftrightarrow F^-$	0.0

2.2 Depletion-driven thermochemistry in the Molten Salt Reactor Experiment

To better understand the problem of depletion-driven thermochemistry, it is helpful to review the first comprehensive operational example of an MSR---the Molten Salt Reactor Experiment (MSRE). The MSRE was a fluoride salt reactor that operated in Oak Ridge National Laboratory (ORNL) in the 1960s for over 11,500 equivalent full-power hours using both ^{235}U- and ^{233}U-based fuel dissolved in the molten salt (Haubenreich and Engel, 1970). The reactor was considered a successful proof of concept of liquid fuel technology, showcasing the benefits of such a design as well as identifying the remaining technical challenges that must be resolved by future research.

Of note for this present work, the implementation of chemistry control of the fuel-salt was a critical aspect of the reactor operation. It was anticipated that structural materials present in the Hastelloy N alloy used for the reactor vessel and piping would reduce UF_4 to UF_3 to some limited extent forming soluble corrosion products in the fuel salt as seen in Eq. 4, where the corrosion of chromium into the fuel salt is highlighted (Shaffer, 1971).

$$Cr^0_{(s)} + 2UF_4 \leftrightarrow 2UF_3 + CrF_2 \tag{4}$$

Therefore, the molten salt system at thermodynamic equilibrium should be "poised" or "buffered" by the UF_4-UF_3 redox couple and a small amount of CrF_2 should be present. However, as UF_4 and UF_3 are consumed and transmuted during depletion, the total amounts and ratio of this redox couple change. If they change sigfnificantly enough, then the system could be increasingly poised or buffered by another redox couple.

In the case of the system shifting towards an oxidizing state where the UF_4 to UF_3 ratio is large or increasing, then the redox couple $Cr_{(s)}$-CrF_2 becomes dominant and poises/buffers the system. This system would then be in an active state of corrosion, where thermodynamic equilibrium is dependent on the amount of $Cr_{(s)}$ that could be extracted from the structural surfaces in contact with the fuel salt. On the other hand, if the system shifts towards a reducing state where the UF_4 to UF_3 is small or decreasing, then the redox couple UF_3-$U_{(s)}$ would become dominant and poise/buffer the system, and uranium would solidify and precipitate out of the fuel salt due to a lack of fluorine potential.

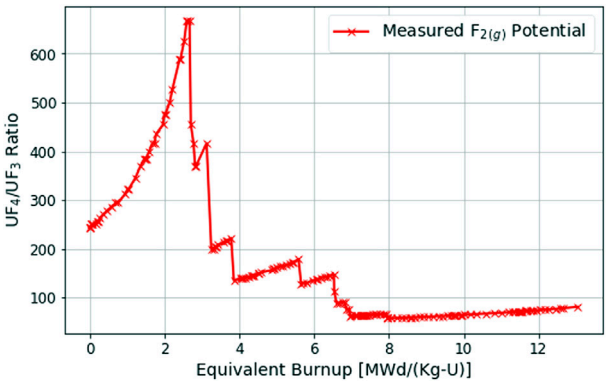

FIGURE 1
UF_4 to UF_3 ratio during the ^{235}U MSRE runs—reformatted from (Thoma, 1971).

2.2.1 Understanding relative redox potentials of reactions

To illustrate this point more clearly, a standard half-cell redox potential table calculated from the MSRE is reproduced here as Table 1 (Baes, Jr, 1965). This table lists the standard half-cell electrochemical redox potentials calculated in FLiBe salt in relation to the fluorine chemical potential where the standard half-cell potential is defined by Eq 3. It is important to note that these redox potentials shown in Table 1 are standard at 1,000 [°K] whereas traditional standard cell potentials by definition mean that the voltage is measured or calculated at 298 [K], 1 [atm], and 1 [M] or $1.0E^{-3}$ [mol/cm^3] solutions. Since these ionic melts would not be liquid at 298 [°K], the standard potentials are calculated at 1,000 [°K] instead, and the other standard states (i.e., pressure and chemical activity) remain the same.

The redox potential of a reaction not at standard states (i.e., redox potentials not calculated or measured at 1,000 [°K], 1 [atm], and $1.0E^{-3}$ [mol/cm^3] solutions) can be calculated by the Nernst equation shown in Eq 5 (Zhang et al., 2018). Here E is the redox potential of the reaction at non-standard states, E^O is the standard cell potential of the complete reaction (i.e., the addition of two half-cell reactions shown in Table 1), and Q is the reaction quotient, which is a ratio of the relative chemical activities of the products to the reactants in the reaction.

$$E = E^O - \frac{RT}{nF} ln(Q) \tag{5}$$

Building upon this point then, the standard redox potential half-cell reactions in Table 1 show the relative likelihood of different reactions happening at different redox potentials with the implicit notion that the chemical activity of the elements being dissolved in the FLiBe salt are all equal to $1.0E^{-3}$ [mol/cm^3]. However, it should be stressed to the reader that the redox potential of reactions depend heavily on the chemical activities of the products and reactants of the reactions as seen in the Q term of Eq 5. Therefore, the relative redox potentials of reactions in a real MSR system made up of base salt elements, fuel, fission products, and corrosion products is not as linear as the table may suggest and that a plethora of reactions shown (and more not shown) in Table 1 will be at various Q values for a given redox potential depending on the chemical activities of the elements in the fuel salt.

As can be at the top of Table 1, the most stable ions are the base salt ions Li^+ and Be^{2+} in addition to a host of rare-earth fission product ions. The low redox potential values of these reactions means that it takes a very limited fluorine potential to sufficiently dissolve these elements in the molten salt, or that they readily form ion pairs with fluorine. Whereas for more positive redox potential values, a larger fluorine chemical potential is required to dissolve these elements in the molten salt.

As discussed earlier, if the redox potential is buffered or poised by the U^{4+}-U^{3+} (UF_4-UF_3) pair in the salt as seen in Eq 4 (i.e., their chemical activities are thermochemically dominant in dictating the fluorine chemical potential), then the redox potential of the fuel salt at thermochemical equilibrium is held somewhere below −3.915 [V]. Therefore, more positive redox potential reactions further down Table 1 will not be significant (i.e., corrosion of $Cr_{(s)}$, $Fe_{(s)}$, and $Ni_{(s)}$ is controlled).

As uranium fissions however, the relative chemical activities of the U^{4+}-U^{3+} buffer pair is sufficiently altered, and the redox potential shifts towards the next thermochemically favorable buffer pair. The resulting two FPs generated in the fuel salt have an aggregated electrochemical potential that is more positive than the single uranium atom they replace and hence, the electrochemical potential of the system increases or becomes more oxidizing (Baes, Jr, 1974). Moving down Table 1 if the chemical activity of $Cr_{(s)}$ in the structural material alloy in thermodynamic equilibrium with the salt is large enough, then the $Cr_{(s)}$-Cr^{2+} will become the dominant redox potential buffer pair and the redox potential of the fuel salt will be held somewhere below to −3.261 [V].

If fluorine has a less negative chemical potential, then UF_4 is overly dominant, and the formation of corrosion products will occur as seen in Eq 4 when the $Cr_{(s)}$-Cr^{2+} buffer becomes dominant. If the fluorine potential continues to increase, then in addition to significant corrosion of structural materials leaching $Cr_{(s)}$, $Fe_{(s)}$, and $Ni_{(s)}$ into the fuel salt, $UF_{5\ (g)}$ and $UF_{6\ (g)}$ gas (not shown in Table 1) will eventually form as well.

2.2.2 Changing redox potential in the MSRE

The chemical activity ratio of UF_4 to UF_3 can be utilized to understand the current redox potential of the fuel salt and was therefore the primary method used to determine the chemical state of the fuel salt during the MSRE as seen in Figure 1 (Thoma, 1971). Ideally, the fluorine potential of the fuel salt would be actively controlled and held steady during reactor operation so that corrosion rates and FP behavior in the fuel salt would be predictable.

However, as seen in Figure 1, the redox potential of the fuel-salt during the MSRE did not remain steady during the entire reactor operation (Thoma, 1971). During the first ~2000 full power hours (or ~2.5 MWd/Kg-U burnup) of the MSRE, the UF_4/UF_3 ratio rose without active chemistry control. This experimental data showcases how, as depletion occurs, the chemical environment of the fuel salt becomes more oxidizing where the fluorine chemical potential increases over time.

Another way to understand this process is that fuel salt develops a cationic charge deficiency due to depletion as dissolved uranium metal is consumed and the FPs that are generated are not as thermochemically stable in fluorides as the original uranium fuel (i.e., noble metal and noble gas FPs Mo, Tc, Xe, Kr) and do not form ion pairs with fluorine (i.e., their cationic charge = 0). To fill this cationic charge deficiency or to satisfy the increased fluorine chemical potential, the chemical reaction in Eq 4 comes into effect to form a new thermochemical equilibrium with a significant amount of corrosion products that have leached into the fuel salt from structural materials in direct contact with the fuel salt.

To limit corrosion, another possibility to reduce the redox potential of the fuel salt is to replace the cationic charge deficiency that develops due to depletion with a more thermochemically stable metal higher up Table 1 (e.g., more U or Be) as seen in Eq 6. In this case the chemical activity of the $Be_{(s)}$-Be^{2+} buffer ratio becomes thermochemically dominant and dictates the fluorine potential.

$$Be^{0}_{(s)} + 2UF_4 \leftrightarrow 2UF_3 + BeF_2 \tag{6}$$

This is exactly what is occurring in Figure 1 when the UF_4/UF_3 ratio sharply decreases---the MSRE fuel salt is being actively reduced through the dissolution of Be into the fuel salt. This process was monitored by taking a fuel-salt sample at an interval of several days to determine the UF_4/UF_3 ratio, before the beryllium rod was be immersed into the fuel salt for a period of a few hours (Thoma, 1971).

2.3 Current state of the art and objective of work

As can be seen from the example of the MSRE, depletion-driven thermochemistry is an integral part of MSR behavior that must be modeled, measured, and controlled in future MSR designs. A survey of existing work in this area to identify the current state of the art will now be provided.

2.3.1 Literature review of similar works

The original research marking the onset of this topic is, of course, the experience of the MSRE identified in the previous subsection (Thoma, 1971). Additionally, in preparation for the proposed Molten Salt Breeding Reactor (MSBR), a simple study of the chemical consequences of fission was performed. The combination of assumed equilibrium oxidation states of FPs and their fission yields were calculated to determine an effective rate of cationic charge deficiency growth (Baes, Jr, 1974). Similarly, the same sort of cationic charge deficiency rate determination using equilibrium oxidation state assumptions of FPs in chloride salts was also performed (Chasanov, 1965). These studies aimed at estimating the amount of extra cationic charge needed to avoid significant corrosion during the operation of the MSRs at higher power.

Recent efforts build upon computational methodology advancements in thermochemistry such as the use of large thermochemical databases and the Calculation of Phase Diagrams (CALPHAD) method (McMuray et al., 2018). In support of these efforts, a new database for chemical analysis of MSRs (e.g., depletion-driven thermochemistry), the MSTDB-TC was developed (Ard et al., 2022). It uses the Modified Quasi-chemical Model in Quadruplet Approximation (MQMQA) for modeling molten salts that can be leveraged by the GEM solver Thermochimica (Poschmann et al., 2021).

These initial efforts culminated in the multiphysics coupling of Thermochimica using the MSTDB-TC in the Virtual Environment for Reactor Applications (VERA) tool suite (Graham et al., 2021). This multiphysics capability included thermal hydraulics in order to provide a temperature-informed spatial thermochemical solution of the MSR system at equilibrium. However, this work did not incorporate depletion and a time evolution of the fuel salt chemistry was not performed.

A parallel effort that utilized the Transient Simulation Framework of Reconfigurable Models (TRANSFORM) was also coupled with Thermochimica using the MSTDB-TC to perform dynamic mass accountancy during various reactor operational transients (Poschmann et al., 2022). This effort resulted in the transient analysis of volatile species formation and extraction into an off-gas system, as well as the freezing and precipitation of molten salt chemical constituents. However, this work did not focus on modeling depletion (i.e., chemical composition) driven thermochemistry changes, but rather focused on temperature effects.

Even more recently, the issue of depletion driven thermochemistry or chemistry-integrated fuel evolution was highlighted by the U.S. DOE's Advanced Reactor Technology–Molten Salt Reactor Program (MSRP) (Shahbazi, 2022a). An excellent and thorough review of thermochemical modeling for radionuclide speciation in molten salts was completed and is highlighted here by the authors for the inquisitive reader (Shahbazi et al., 2021). Lastly, radionuclide species transport in the MSRE was conducted albeit without coupling depletion and thermochemistry in the analysis (Shahbazi et al., 2022b).

2.3.2 Objective of present work

The objective of this present work is to use the same methodology framework of MSR multiphysics analysis as identified in the literature review and apply this approach to model depletion-driven thermochemistry of MSRs using the DOE's NEAMS toolkit built on the Multiphysics Object-Oriented

Simulation Environment (MOOSE) framework (Martineau, 2021). This approach offers a greater flexibility of multiphysics and multiscale modeling capability, where other MOOSE based physics models for thermal-hydraulics, species mass transport, and corrosion can be easily incorporated in the future. Additionally, this work will mainly focus on modeling the changing redox potential of both fluoride and chloride salts as they undergo depletion and active chemistry control. Consequentially, this work will identify the remaining thermochemical data and modeling methodology challenges that are needed to comprehensively model depletion-driven thermochemistry in MSRs.

This present work is built upon smaller pieces that were previously published by the authors as key milestones in developing this depletion-driven thermochemistry analysis capability using NEAMS tools. Notably, the depletion solver in the neutronics code Griffin had to be altered to account for nuclide removal and multi-region depletion (Walker et al., 2022). Most recently, the coupling of Thermochimica using the MSTDB-TC with Griffin was performed to model material accountancy of gaseous species being extracted into the off-gas system (Walker et al., 2023). This work builds upon these initial steps to perform tightly coupled depletion-driven thermochemical analyses of MSRs focusing on the changing redox potential and the implementation of active redox control mechanisms.

3 Computational methodology and numerical implementation

This section details the computational methodology and numerical implementation of the multiphysics coupled code simulation capability developed for this analysis. Since much of this development work was done in previous reports documenting the incremental steps of this capability, readers are encouraged to review these for more details (Walker et al., 2022; Walker et al., 2023). A brief description for each individual code as well as the coupled system will be provided. Lastly, the current capabilities and limitations of the MSTDB-TC are identified for this work.

3.1 Griffin

Griffin is a NEAMS tool used for multi-fidelity neutronics and fuel depletion. Recent efforts incorporated a nuclide removal and multi region microscopic depletion capability for modeling off-gas and other waste streams in MSR systems during burnup (Walker et al., 2022).

The depletion equation solved by Griffin, also known as the Bateman equations, track the nuclide number density of the fuel and resulting FPs, and incorporates fission, neutron transmutation, and radioactive decay as seen in Eq 7 has additional terms not traditionally seen in the Bateman equations, which represent sources and sinks from removal waste streams and from chemical reactions at interfaces.

$$\frac{dN_Z^A(t)}{dt} = \sum_{Z',A'=1}^{M}\left(\gamma_Z^A\sum_{g=1}^{G}\sigma_{f(Z',A'),g}(t)\phi_g(t) + \sum_{g=1}^{G}\sigma_{(Z',A')\to(Z,A),g}(t)\phi_g(t) + r_{(Z',A')\to(Z,A)}\lambda_{Z'}^{\mathring{A}}\right)N_{Z'}^{\mathring{A}}(t) - \lambda_Z^A N_Z^A(t) - \sum_{g=1}^{G}\sigma_{a(Z,A),g}(t)\phi_g(t)N_Z^A(t) - f_{chem,Z}^A(t) - f_{stream,Z}^A(t) \tag{7}$$

Here $N_{Z'}^{\mathring{A}}(t)$ is the number density of other nuclides with atomic number Z' and mass number A', which produce nuclide $N_Z^A(t)$, γ_Z^A is the fission yield of nuclide N_Z^A from $N_{Z'}^{\mathring{A}}(t)$, $\sigma_{f(Z',A'),g}(t)$ is the groupwise microscopic fission cross section of $N_{Z'}^{\mathring{A}}(t)$, $\phi_g(t)$ is the groupwise scalar neutron flux, $\sigma_{(Z',A')\to(Z,A),g}(t)$ is the groupwise microscopic transmutation cross section of $N_{Z'}^{\mathring{A}}(t)$ that produces $N_Z^A(t)$, $r_{(Z',A')\to(Z,A)}$ is the branching ratio for radioactive decay, $\lambda_{Z'}^{\mathring{A}}$ is the radioactive decay constant for $N_{Z'}^{\mathring{A}}(t)$, λ_Z^A is the radioactive decay constant for $N_Z^A(t)$, $\sigma_{a(Z,A),g}(t)$ is the groupwise absorption cross section for $N_Z^A(t)$, $f_{chem,Z}^A(t)$ is a chemical reaction source at interfaces, and $f_{stream,Z}^A(t)$ is a mass transfer removal source term for feed and waste streams.

The primary application of this work focuses on utilizing the $f_{stream,Z}^A(t)$, where nuclides will be withdrawn or added to the reactor system which alters the ongoing depletion of the fuel and nuclide inventory. By altering the $f_{stream,Z}^A(t)$ term, the chemical composition changes and this will drive any observed thermochemical equilibrium changes in the fuel salt. The form $f_{stream,Z}^A(t)$ takes is defined in Eq 8, a type of effective removal rate that depends on the existing amount of the nuclide in the fuel salt and a feed rate L, where L can be positive or negative for material additions or subtractions from the system.

$$f_{stream,Z}^A(t) = LN_Z^A(t) \tag{8}$$

3.2 Thermochimica

Thermochimica is the GEM that is currently being incorporated into the MOOSE framework for use in many NEAMS tools for thermochemistry analyses. The reader is encouraged to investigate the references in this section for more details involving the specific methodologies used to model the thermochemistry of ionic liquids. A high-level overview of this detailed subject is provided here.

Thermochimica uses the CALPHAD method and, for this case, the MSTDB-TC database to determine the equilibrium of an isothermal and isobaric system by minimizing the global Gibbs free energy of the chemical composition of the system. Eq 9 shows the general form of the Gibbs energy of the system where G^{ref} is the reference Gibbs energy, T is the temperature, ΔS is the change in configurational entropy, and G^{XS} is the excess Gibbs energy (McMuray et al., 2018).

$$G = G^{ref} - T\Delta S + G^{XS} \tag{9}$$

The G^{XS} term accounts for the non-ideal mixing that arises from chemical species interactions occurring in the system. In an ideal gas, the G^{XS} term is negligible, but this is not the case for ionic liquids like molten salts. This is where the MQMQA comes in handy to accurately characterize the chemical species interactions that occur in molten salts to determine the effect of non-ideal mixing (Poschmann et al., 2021).

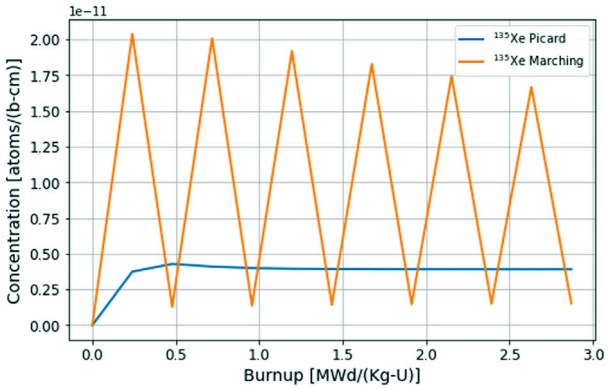

FIGURE 2
Comparison of ^{135}Xe core concentration using a time marching scheme *versus* a Picard iteration scheme.

Using the MQMQA and an extensive experimental thermochemical database, Thermochimica can proceed to solve Eq 9 and determine equilibrium phase values and chemical potentials of species in the molten salt. The MSTDB-TC database funded by the U.S. DOE contains one of the largest collections of self-consistent and vetted fluoride and chloride thermochemical data (Ard et al., 2022).

Utilizing the MSTDB-TC within Thermochimica allows for the thermochemical equilibrium of the fuel salt to be calculated at each depletion step. In addition to understanding how the chemical potentials of species change due to composition changes in the fuel salt, vapor pressures of chemical species in the fuel salt can also be calculated for volatilization and off-gas extraction analysis.

3.3 Multiphysics coupling schemes and numerical performance

This section examines the multiphysics coupling scheme used between Griffin-depletion and Thermochimica. Initially, a loosely coupled (or time-marching) scheme was implemented, with each code calculating one solution for each given time step. Although this served as a proof of concept for the depletion-driven thermochemistry capability, a more accurate coupling scheme was needed as oscillatory solutions were obtained for volatile isotopes with large extraction rates as seen in Figure 2. Figure 2 showcases the changing concentration of ^{135}Xe in the reactor core during depletion where volatile species and noble gases are being extracted to an off-gas system using a user specified system mass transfer coefficient L as seen in Eq 8. The time marching multiphysics coupling scheme incorrectly overpredicts and underpredicts the solution marked by the orange sawtooth in Figure 2.

The current tightly coupled implementation uses Picard iterations, with the two individual codes iterating their solutions until both solutions stop changing within a given tolerance as seen in Figure 3. Here the driving application is Griffin-depletion since it defines the fuel-salt composition needed by Thermochimica to determine the equilibrium thermochemistry of the system. Griffin calculates the nuclide inventory A at time step t^{n-1} and passes this to Thermochimica which calculates the thermochemical equilibrium of the fuel salt and determines the feed rate $f^{A}_{stream,Z}$ at time t^{n-1} by accounting for the mass transport of volatile species. A time step is taken to time step t^{n} where a new nuclide inventory A and a new feed rate $f^{A}_{stream,Z}$ are calculated. The average of the two feed rates $f^{A}_{stream,Z}n-1$ and $f^{A}_{stream,Z}n$ is used to re-calculate the original time step t^{n-1} until both solutions self-consistently converge to a set tolerance.

To illustrate how Thermochimica alters the nuclide inventory calculation done by Griffin, a truncated Thermochimica output example is provided in Table 2 which describes what sort of chemical species are present in the liquid fuel salt and the vapor pressures of these species if the salt is in contact with an off-gas system liquid-gas interface.

At this point a user specified system mass transfer coefficient L as seen in Eq. 8 can be used to extract fractions of the vapor pressure of gaseous species to an off-gas system which will determine the nuclide inventory calculated in Eq 9 as seen in Figure 3. The system mass transfer coefficient L which details the mass transfer to the

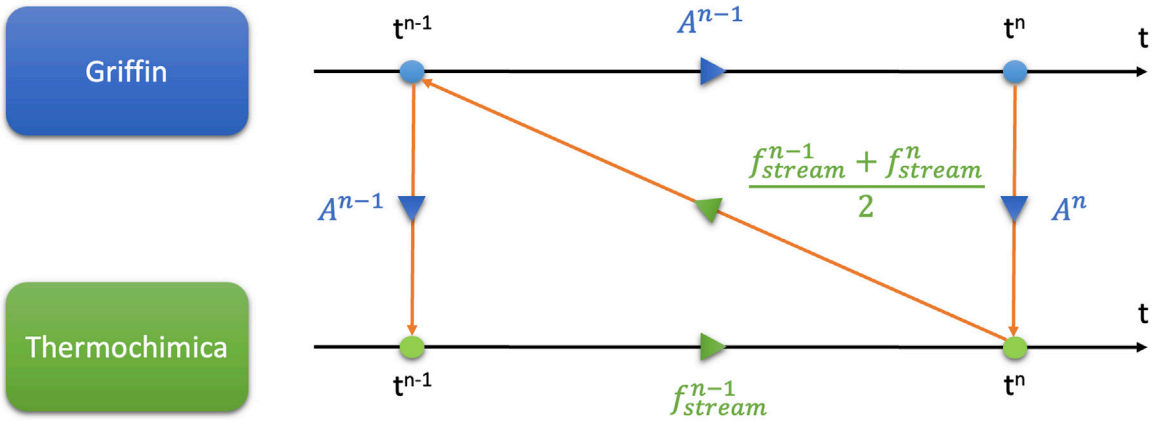

FIGURE 3
Griffin and Thermochimica multiphysics coupling scheme.

TABLE 2 Truncated Thermochimica Output Example to Determine $f^{A}_{stream,Z}(t)$

	Ionic Endmembers in Molten Salt Fluoride Liquid [mol]	Vapor Pressure of Gaseous Species [atm]
Fluoride Fuel Salt at 2.87 [MWd/Kg-U]	$LiF-6.48e^{+04}$	$LiF-3.83e^{-08}$
	$BeF_2-7.75e^{+03}$	$Li_2F_2-1.10e^{-08}$
	$UF_4-8.72e^{+02}$	$BeF_2-3.73e^{-06}$
	$UF_3-2.84$	$LiBeF_3-9.43e^{-07}$
	$PuF_3-4.82e^{-01}$	$RbI-2.10e^{-08}$
	$RbF-6.17e^{-02}$	$CsI-2.99e^{-08}$
	$CsF-1.22e^{-01}$	$Li_3F_3-3.36e^{-09}$
	$CsI-5.95e^{-07}$	$UF_4-1.52e^{-09}$
	$RbI-3.13e^{-07}$	$LiI-9.11e^{-09}$
	$LiI-1.68e^{-02}$	$I-2.07e^{-09}$

liquid-gas interface of an off-gas system should be determined by higher fidelity spatially resolved chemical species distributions in the reactor system (Tano, 2023a).

There are two primary assumptions that are made in this coupled multiphysics methodology that must be made evident. One is that the multiphysics solution is pointwise, or zero dimensional, where the reactor fuel-salt system is homogenized, and the spatial temperature or fuel-salt composition distributions are not accounted for in this analysis. Therefore, this proof-of-concept analysis provided here assumes a system mass transfer coefficient L for the 0-D system rather than calculating it from a spatially resolved thermal-hydraulic solution. Additionally, this methodology assumes that the changes in the overall fuel salt composition due to depletion is a slow process and that the system is always in thermochemical equilibrium. For most nuclides which make up the elements in the molten salt this is a good assumption and the nuclides which are changing rapidly due to radioactive decay make up a negligible fraction of the element or total chemical composition.

For fast changes in the chemical composition, which occur during active redox potential control, a chemical redox kinetics model for corrosion and reduction at interfaces would be required to model the time and spatial effect of this process (Walker and Ji, 2021b; Tano, 2023b). The analysis of active redox potential control provided in this work will be stepwise accounting for the chemical potential before and after the fuel salt composition has been altered.

3.4 Discussion of current MSTDB-TC capability and limitations

Before diving into the results section, it is important to preface the results with a discussion of the database that was used, as well as the current limitations restricting the applicability and scope of this current analysis. The most up to date MSTDB-TC version at the time this work has been completed was MSTDB-TC V2.0, which was used in Thermochimica. It is important to note that the formal process of compiling these self-consistent thermochemical databases is a rigorous, time-consuming process which can become even more difficult as new species, elements, and their respective interactions are added (Ard et al., 2022).

As a result, the current version of the MSTDB only contains 16 elements for both fluoride and chloride salts as seen in Table 3. The respective fluoride and chloride databases differ in significant ways, the most obvious being the base elements of the ionic salts (i.e., Li, Be, F, Na, K, and Ca for fluoride salts, and Li, Na, Mg, Al, Cl, K, and Ca for chloride salts). Other differences are that the fluoride database includes more rare earth element FPs (i.e., La, Ce, and Nd), while the chloride database includes more corrosion product elements (i.e., Cr, Fe, and Ni). Lastly, both the databases include Cs and I. The chemical behavior of these elements is important due to their radiological effect on humans and are therefore important from a source term or safety perspective.

While these databases may be well suited for thermochemistry calculations of fuel salt behavior at the beginning of life of the reactor, they are not yet able to completely capture the role of depletion in altering the redox potential, due to missing key FPs that are expected to interact with the base ion (F or Cl) and form ionic end members in the fuel salt. However, it should be noted that the importance of this effect will depend on the oxidation state and the relative chemical activity of these FPs (Chasanov, 1965; Baes, Jr, 1974). Thus, for low burnup, the current elements available in the MSTDB database are enough to demonstrate the general chemical evolution of MSRs due to depletion.

A few of these important corrosion and fission products currently missing from the MSTDB-TC are also listed in Table 3. Table 3 lists key FPs that buildup in non-negligible amounts after considerable depletion (Zr, Nd, Mo), which are important for determining the redox potential of the fuel salts towards the end of the reactor lifetime. Most important for fluoride salts is the inclusion of corrosion products Cr and Fe in the system since the chemical activity of $Cr_{(s)}$-CrF_2 will poise the redox potential after the UF_4/UF_3 ratio becomes too oxidizing as seen in Eq 4; Table 1 (Besmann and Schorne-Pinto, 2021).

It is important to note that, though the behavior of Mo in both salts is still being determined, it is likely insoluble and chemically neutral as a noble metal in fluoride salts during normal fluorine potentials poised by the UF_4/UF_3 couple, whereas it is believed to be

TABLE 3 MSTDB-TC V2.0 Analysis.

	Available Elements	Important Corrosion and Fission Products not in MSTDB-TC V2.0
Fluoride Salts	Li, Be, F, Na, K, Ca, Ni, Rb, I, Cs, La, Ce, Nd, Th, U, Pu	Cr, Fe, Zr, O, H
Chloride Salts	Li, Na, Mg, Al, Cl, K, Ca, Cr, Fe, Ni, Rb, I, Cs, Ce, U, Pu	Nd, Zr, Mo, O, H

soluble with a valence state of +3 for chloride salts during normal chlorine potentials (Thomas and Jerden, 2020). Here a "normal" fluorine potential is one poised by the UF_4-UF_3 couple as seen in Figure 1 where an ideal UF_4/UF_3 ratio is somewhere between 10 and 100 to limit corrosion (Guo et al., 2017) where the fluorine potential of the initial fuel-salt composition is maintained. A normal chlorine potential similarly would be one that is poised by the UCl_4-UCl_3 couple. For a corresponding electrochemical potential plot of Table 1 for chemical species in a molten chloride salt, the reader is advised to review (Guo et al., 2018). Lastly, note that elements involved in oxidation reactions from air or water (i.e., H and O) are currently excluded, and likely play an important role in altering the redox potential during initial or operational air and moisture ingress (Thoma, 1971).

Due to these thermochemical data shortcomings, it is anticipated that the multiphysics depletion-driven thermochemical analysis of MSRs in its current capability will not capture the evolving redox potential of the fuel salt in an absolute sense. Rather these calculations serve as a proof of concept of the multiphysics depletion-driven thermochemistry capability that will be validated against real fuel-salt systems as more vetted thermochemical data is added to the MSTDB-TC. A prime example of this would be to use the chemical data from the MSRE during the ^{235}U runs (Thoma, 1971); this future work can be conducted once Zr (a primary fuel-salt component in the MSRE) is added to the MSTDB-TC.

4 Results: Depletion-driven thermochemical analysis of molten salt reactors

This section presents some key results obtained using the multiphysics-coupled, depletion-driven thermochemistry scheme detailed in the previous section. First, the specifications of the generic zero-dimensional fluoride and chloride MSRs are defined. The following subsections detail the changing fluorine and chlorine potential of the systems as they undergo depletion. Vapor pressures for chemical species in both systems are also calculated throughout burnup. Finally, active redox chemistry control is modeled, and the resulting changing thermochemical equilibrium of the fuel-salt is calculated.

4.1 Specification of fluoride and chloride zero-dimensional MSR systems

This subsection examines the specifications of two generic zero-dimensional fluoride and chloride salt reactors used in this analysis. These are hypothetical use cases that are leveraged to evaluate possible depletion-driven thermochemical effects during burnup.

Table 4 identifies the specifications used in the depletion-driven thermochemical analysis of these two generic reactor types. The fluoride salt composition was selected to be close to that of the MSRE fuel salt with the notable exception that the Zr component is missing as mentioned earlier (Thoma, 1971). Instead, it is very similar to pure FLiBe (2LiF-BeF_2) salt with the replacement of some beryllium with uranium fuel. Additionally, the ^{235}U enrichment of the system was set to 33.3% to match the MSRE fuel salt.

The chloride salt composition on the other hand is a chloride eutectic fuel salt originally proposed for fast chloride breeder reactors (Mourogov and Bokov, 2006). Simply put, this is molten table salt with some uranium fuel mixed in. Both the power densities and uranium enrichments are set equal so that the depletion histories can be compared between the two fuel-salt systems (i.e., the amount of uranium fuel consumed in both reactors is the same).

Due to the thermochemical data limitations discussed in the previous section, a low burnup of 2.87 [MWd/Kg-U] is chosen for both reactors. To simplify the analyses, a constant scalar neutron flux is chosen, and one condensed energy group is used to evaluate the mid-burnup micro cross sections of nuclides in the reactor as seen in (Walker et al., 2022; Walker et al., 2023) for both fluoride and chloride systems. Here the Monte Carlo code SERPENT-2 is used to generate the micro cross sections and to collapse the neutron flux into a single energy for both generic reactor systems (Aufiero et al., 2013; Walker et al., 2022).

4.2 Changes in redox potential due to depletion

This subsection investigates changes in the chemical fluorine and chlorine potential along with their associated electrochemical redox potentials due to depletion. It is important to note that these sets of calculations do not include any active redox control measures; so, the expected behavior of the redox potential should increase or become more oxidizing during depletion as observed in the MSRE (Thoma, 1971) and predicted for chloride systems (Chasanov, 1965).

4.2.1 Fluoride fuel salt analysis

The results of the multiphysics depletion-driven thermochemistry analysis of a fluoride fuel salt using the MSTDB-TC V2.0 during a 2.87 [MWd/Kg-U] burnup and 60 days of operation are presented below. Figure 4 showcases the change in fluorine potential and its associated redox potential where Eq 3 sets the standard half-cell potential.

TABLE 4 Generic Reactor Specifications.

Specifications	Fluoride Reactor	Chloride Reactor
Initial Salt Composition [mol%]	LiF [66.4]–BeF_2 [32.7]–UF_4 [0.9]	NaCl [66.7]–UCl_3 [33.3]
Salt Density [g/cm^3]	1.94	3.13
^{235}U Enrichment [%]	33.3	33.3
Temperature [°K]	936.0	936.0
Pressure [atm]	1.34	1.34
Power Density [kW/cm^3]	0.01	0.01

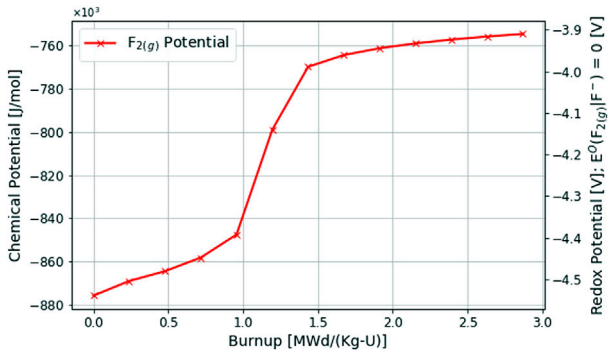

FIGURE 4
Change in fluorine potential over 60 days or 2.87 [MWd/Kg-U] burnup.

Here, the fluorine potential is steadily increasing over the first 1.0 [MWd/Kg-U] of burnup. This indicates that the fuel salt is becoming more oxidizing which is the expected outcome of depletion as observed in Figure 1 for the MSRE, where the UF_4/UF_3 measurement of the redox potential is increasing. Although this analysis is not meant to be a direct comparison with the MSRE since the base MSRE fuel salt is not currently available in the MSTDB-TC V2.0, the redox potential is increasing more rapidly during the first 1 [MWd/Kg-U] of burnup compared with the MSRE in Figure 1. This is especially true when the fluorine potential rapidly increases between 1.0 - 1.5 [MWd/Kg-U] of burnup. Therefore, it is safe to say that the current MSTDB-TC V2.0 overestimates the depletion-driven evolving fluorine potential due to a lack of some important reducing fission products (e.g., Zr) for the fluoride fuel salt system.

The apparent step change in fluorine potential observed from 1.0–1.5 [MWd/Kg-U] of burnup is related to a significant shift in the chemical activity of redox buffers as discussed in Section 2. From 0.0–1.0 [MWd/Kg-U] of burnup, the fluorine potential is controlled by the UF_4/UF_3 redox buffer pair. However, the chemical activity of UF_3 is greatly decreasing as a cationic charge deficiency builds up due to depletion, and the UF_3 is forced to shift towards UF_4 as seen in Eq 4. Eventually UF_3 is depleted, and the redox buffer will shift to the chemical activity ratio of $Cr_{(s)}$-Cr^{2+}. However, in this analysis using the MSTDB-TC V2.0, corrosion/structural products Cr and Fe are not currently available, so the support structure in thermodynamic equilibrium with fuel-salt available to be modeled in this analysis is pure Ni $_{(s)}$ with a chemical activity of 1.0 since there is no alloy. Therefore, the redox potential shifts from being dictated by the chemical activity ratio of UF_4/UF_3 to the new redox buffer $Ni_{(s)}$-Ni^{2+} in this analysis as seen in Eq 10

$$\boldsymbol{Ni^0_{(s)} + 2UF_4 \leftrightarrow 2UF_3 + NiF_2} \tag{10}$$

This shift in redox potential buffers can occur so rapidly in the fluoride fuel salt composition chosen since the relative chemical activity of Uranium is so small in the base fuel salt as seen in Table 4 (i.e., 0.9 [mol%]). The missing chemical activities of key FPs may also be accentuated by the small amount of U contained in the fluoride fuel salt system when compared to the chloride fuel salt system analyzed in the following subsection. From 1.5 [MWd/Kg-U] of burnup onwards, the $Ni_{(s)}$-Ni^{2+} redox buffer poises the system and the fluoride fuel salt is in a state of active corrosion where NiF_2 attempts to replace the cationic charge deficiency generated through depletion (i.e., it tries to take up the excess fluorine potential generated through the generation of less thermochemically stable FPs).

Whereas this is a technically accurate description of the fluoride fuel salt system given the current thermochemical database, it is not necessarily representative of a real MSR system where the structural material is an alloy instead of pure $Ni_{(s)}$. As seen in Table 1; Eq 4, a more physical scenario would be the oxidation of $Cr_{(s)}$ from the alloy materials into the fuel salt (Besmann and Schorne-Pinto, 2021). Therefore, the resulting redox potential calculated here is similarly too high due to missing thermochemical data for Cr and Fe in fluoride salts and should be lower being controlled by the $Cr_{(s)}$-Cr^{2+} buffer instead.

Ongoing development of the MSTDB-TC will likely rectify this issue in the near term (McMurray et al., 2021). The addition of ZrF_4 (a base component of the MSRE fuel salt) and corrosion products CrF_2 and FeF_2 will enable the benchmarking of this multiphysics depletion-driven thermochemistry capability against the UF_4/UF_3 data observed during the MSRE (Thoma, 1971).

Finally, the changing chemical potentials of a select number of elements in the fluoride fuel salt due to depletion are plotted in Figure 5. As seen in red, the fluorine potential is the most negative chemical potential in the system as expected. As the fuel salt is depleted, the chemical potential of all cations (i.e., Li, Be, U, Pu, Cs) decrease to adjust for the increase of the chemical potential of the anions (F and I). The chemical potential of uranium decreases the most compared with other cations since it is being depleted by

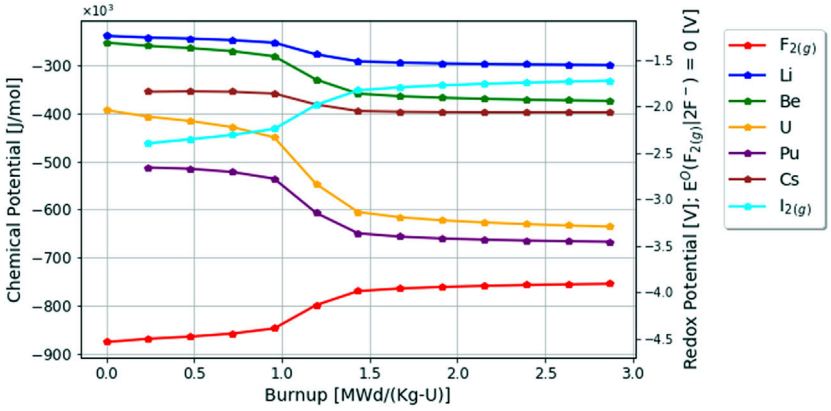

FIGURE 5
Change in chemical potentials in fluoride fuel salt over 60 days or 2.87 [MWd/Kg-U] burnup.

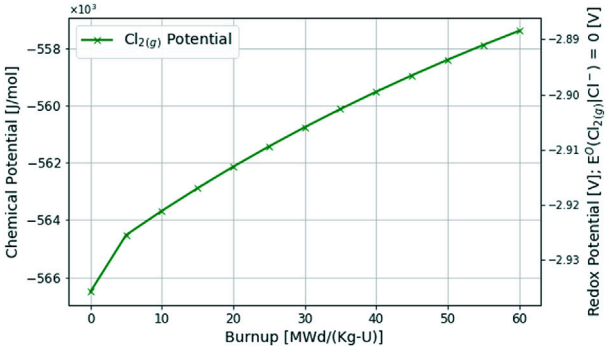

FIGURE 6
Change in chlorine potential over 60 days or 2.87 [MWd/Kg-U] burnup.

fission and is the initial redox buffer until it no longer poises the system, and rapidly decreases as fluorine looks for a more positive redox buffer to consume. Lastly, it is important to note that as the redox potential increases, so does the iodine potential which is an important consideration for vapor pressures and source term calculations as seen in the following subsections.

4.2.2 Chloride fuel salt analysis

The results of the multiphysics depletion-driven thermochemistry analysis of a chloride fuel salt using the MSTDB-TC V2.0 during a 2.87 [MWd/Kg-U] burnup and 60 days of operation are presented below. Figure 6 showcases the change in chlorine potential and its associated redox potential where the standard half-cell potential is defined by Eq 11

$$Cl_{2(g)} + 2e^{-} \leftrightarrow 2Cl^{-},\ E^{O} = 0\ [V] \tag{11}$$

Like the fluoride fuel salt, the redox potential gradually increases, meaning the fuel salt is becoming more oxidizing as anticipated. Unlike the fluoride fuel salt however, there is no acceleration of redox potential occurring meaning the redox buffer in place, likely UCl_4/UCl_3, is dictating the chlorine potential in the fuel salt. Here uranium is a much larger fuel salt constituent compared to the fluoride fuel salt as seen in Table 4 (i.e., 33.3 [mol%]) and therefore the chemical activities of the UCl_4/UCl_3 buffer ratio are more stable. Additionally, this analysis using the current thermochemical database would suggest that the cationic charge deficiency generated from the depletion of UCl_3 is less than the cationic charge deficiency that occurs from the depletion of UF_4.

Most of the key fission and activation products currently accounted for in the MSTDB-TC V2.0 for fluorides form trifluorides or MF_3 (e.g., CeF_3, NdF_3 PuF_3). The fission of UF_4 fuel therefore rapidly yields a significant cationic charge deficiency. Whereas for the chloride salt, the primary fuel is UCl_3, and the key fission and activation products currently accounted for in the MSTDB-TC V2.0 for chlorides also form trichlorides (e.g., $CeCl_3$ and $PuCl_3$). As a result, the rate of cationic charge deficiency is less pronounced for chlorides than fluorides given the current thermochemical database. In other words, based on the current available thermochemical data for fission and activation products included in MSTDB-TC V2.0, the missing charge from UCl_3 consumption (cationic charge of 3+) is less pronounced than the missing charge from UF_4 consumption (cationic charge of 4+).

Since the potential is increasing, there is not enough soluble material for the chlorine to dissolve. Like the oxidizing fluoride fuel salt example, a realistic chlorine fuel salt reactor in thermodynamic equilibrium with the structural material holding the salt will begin to dissolve the structural materials at the wall interfaces forming corrosion products $CrCl_2$ and $FeCl_2$. In this situation, Cr is available for chlorides in the MSTDB-TC V2.0. Like the fluoride fuel salt example where pure $Ni_{(s)}$ was used as the structural material, here a pure $Cr_{(s)}$ structural material with a chemical activity of 1.0 is used instead. Future work will refine this interaction by correctly accounting for the chemical activity of elements in the secondary phase model of the alloy (Besmann and Schorne-Pinto, 2021).

However, since the redox potential of $CrCl_2$ is similar to UCl_3 (i.e., it is the first corrosion product to form in significant amounts as seen in the electrochemical potential plot for chlorides in (Guo et al., 2018)) this is not a terrible approximation. Therefore, the primary

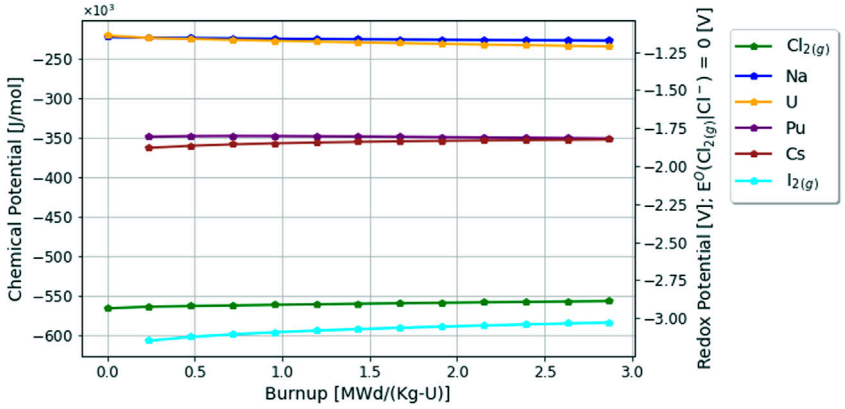

FIGURE 7
Change in chemical potentials in chloride fuel salt over 60 days or 2.87 [MWd/Kg-U] burnup.

and end time effect of corrosion on controlling the redox potential of the fuel salt can be modeled. That being said, the rate of this corrosion is too fast, since the chemical activity of pure $Cr_{(s)}$ is far greater than it would be in an alloy, and the rate of chemical activity of $Cr_{(s)}$ diffusing to the grain boundaries would require a redox kinetics model instead of a thermochemical equilibrium calculation as used in this analysis.

In this analysis, the initial chlorine potential of the chloride fuel salt readily corrodes the pure $Cr_{(s)}$ structural material. This effect also contributes to the diminished change in the redox potential during burnup since the chemical activity of the $Cr_{(s)}$-Cr^{2+} couple entering the fuel salt is significant to nearly replace the cationic charge deficiency generated through less thermochemically stable FPs.

Lastly, the changing chemical potentials of a select number of elements in the chloride fuel salt due to depletion are plotted in Figure 7. As seen in green, the chlorine potential is the quite negative in the system as expected. Of particular interest here, the iodine chemical potential is more negative in the chloride fuel salt than it is in the fluoride fuel salt when comparing Figures 5, 7. Here the decrease in the uranium chemical potential is very minimal compared with the fluoride fuel salt, since the relative chemical activity of uranium in the chloride fuel salt is not changing as rapidly as in the fluoride fuel salt. Lastly, it appears that the chemical potential of cesium, which is important in determining vapor pressures covered in the next section, just so slightly increases over depletion. This is likely an effect of corrosion products entering the fuel salt, since the general behavior of the chemical potential of cations is to go down as the aggregate anion potential increases.

4.3 Changes in vapor pressures of chemical species due to depletion

This subsection focuses on the consequences that a changing redox potential due to depletion will have on the vapor pressure of chemical species in the fuel salts. Both fluoride and chloride salts are analyzed based upon the changing redox potential observed in the previous section.

4.3.1 Fluoride fuel salt analysis

The results for the vapor pressures in the fluoride fuel salt without active redox control are shown in Figure 8. Here the highest vapor pressures are of the base salt constituents (i.e., F, Li, Be, except for U). This is because these elements have the highest partial pressures in the system. The general trend for vapor pressures of minor fission and transmutation product elements is that they increase as their chemical activity builds up in the fluoride fuel salt.

One key item of note for accident source term analysis is that the vapor pressure of iodine in fluoride fuel salts significantly increases when the fluorine potential increases corresponding to Figures 4, 5. Additionally, the vapor pressure of Pu in the fluoride fuel salt shows how extremely stable this element is in fluoride fuel salts also evidenced by its chemical potential in Figure 5.

4.3.2 Chloride fuel salt analysis

The results for the vapor pressures in the chloride fuel salt without active redox control are shown below in Figure 9. Like the fluoride fuel salt analysis, the chloride salt remains quite stable throughout the burnup period as seen in Figure 7, although the redox potential is ever so slightly increasing over the reactor operation period.

As seen previously in Figure 8, the vapor pressures of elements are dictated by their relative concentration in the fuel salt, so base elements Cl, Na, and U have the highest vapor pressures in Figure 9. However, as the fuel salt becomes more oxidizing due to the rising redox potential, the rise in uranium volatility despite its declining chemical activity can be observed. In contrast to the fluoride salt, most of the elements are typically less stable in the chloride salt when comparing Figures 8, 9 due to the difference in the higher electronegativity of fluorine vs. chlorine. One last interesting item to note is that iodine is apparently more stable in chlorides than fluorides, whereas cesium has roughly the same stability in both; this is an important understanding when considering chemical speciation during accident scenarios.

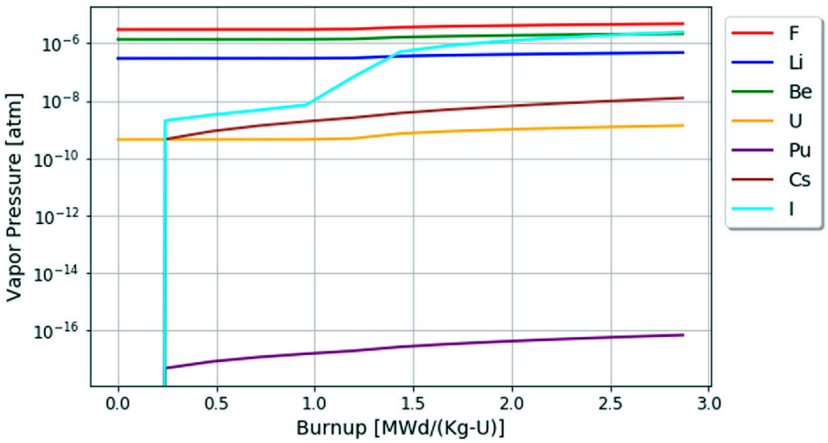

FIGURE 8
Changes in element vapor pressures in the fluoride fuel salt over 60 days or 2.87 [MWd/Kg-U] burnup.

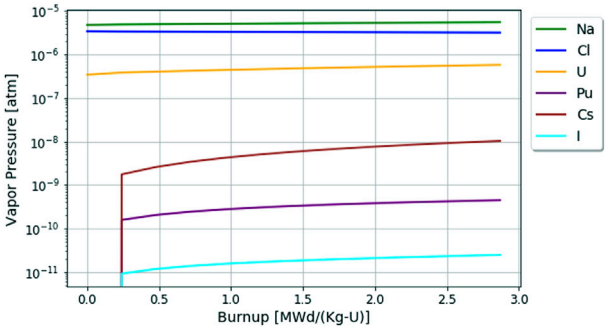

FIGURE 9
Changes in element vapor pressures in the chloride fuel salt over 60 days or 2.87 [MWd/Kg-U] burnup.

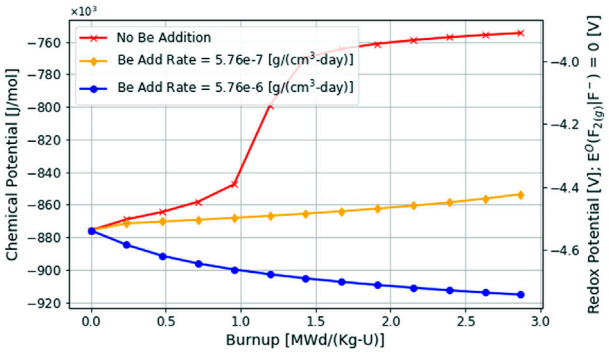

FIGURE 10
Change in fluorine potential with active redox potential control.

4.4 Depletion-driven thermochemistry with active redox potential control

Lastly, the following analyses model scenarios where the chemistry in the MSR system is being actively controlled during operation. As mentioned previously, if the molten salt becomes more oxidizing over time as expected and seen during the MSRE, the redox potential is actively controlled by adding a reducing metal to the molten salt.

4.4.1 Fluoride fuel salt analysis

As seen in the MSRE and in the results of the previous analyses, the fluorine potential increases due to depletion. To maintain a well-behaved reactor and minimize the acceleration of corrosion, the MSRE would periodically reduce the redox potential of the salt by adding a reducing metal to the fuel-salt, typically Be as seen in Eq. 6 (Thoma, 1971; Kelleher et al., 2016). There are several methods for controlling the redox potential as identified here (Zhang et al., 2018). Actively controlling the redox potential through beryllium addition can be modeled using the new multiphysics depletion-driven thermochemistry capability and is illustrated in Figure 10.

Here the L term in Eq 8 is utilized to feed beryllium into Eq 7 thereby controlling the redox potential of the system. As shown in the plot, the beryllium additions can control the redox potential as depletion proceeds. The redox potential looks much smoother when comparing against Figure 1 from the MSRE, because the simulation assumes a constant, continuous rate of beryllium addition whereas the MSRE gradationally added beryllium to reduce the redox potential.

It should be stressed that Figure 10 is not modeling a beryllium rod constantly being dissolved in the fuel salt. This type of analysis would require a redox kinetics model; subsequently if a large enough amount of beryllium was constantly available to dissolve into the salt, it would result in the fuel salt eventually being over-reduced and thereby precipitate solid uranium fuel as seen in Table 1 and can be inferred from the fast reduction that occurs in Figure 1. Instead, Figure 10 is modeling a discrete, constant rate of beryllium addition. A controlled specific mass of the material is being introduced to the system. In an ideal situation, a constant *in situ* redox potential measurement would be implemented, with a controller constantly

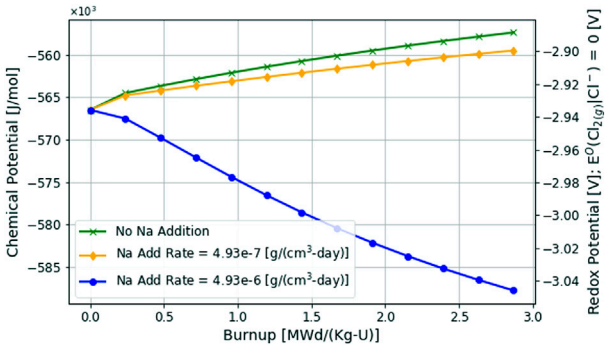

FIGURE 11
Change in chlorine potential with active redox potential control.

monitoring the potential and raising or lowering a beryllium rod into the salt to balance the chemical state as depletion proceeds.

4.4.2 Chloride fuel salt analysis

Like the fluoride fuel salt analysis, the chloride fuel salt can also be controlled through reducing metal additions. The results for sodium additions to the chloride fuel salt can be seen in Figure 11. Here, sodium additions can serve the same purpose as the beryllium additions in the fluoride fuel salt. The reducing metal can help control or reduce the redox potential of the fuel salt during depletion. This reaction with a more thermochemically stable metal would then be dominant in absorbing excess chemical potential and would thereby limit the corrosion that the MSR system may experience. The discrete constant rates of sodium additions are shown in Figure 11 In both fluoride and chloride systems, the possibility of over-reducing the salt as seen in the blue circle marked lines in Figures 10, 11 can be a valid concern depending on the choice of reducing metal or redox control method that is used (Zhang et al., 2018; Newton et al., 2020).

4.5 Future improvements to the model

This research provides an initial starting point to build a complex multiphysics framework for species tracking simulation inside MSRs. This first step consisted of incorporating depletion-driven thermochemistry within the NEAMS framework. This effort will be steadily and continuously enhanced to incorporate higher levels of fidelity. Logical next steps to enhance this capability include coupling depletion-driven thermochemistry with thermal hydraulics so that the impact of advection can be captured as well as provide a multi-dimensional resolution of the system.

Parallel work has already laid the foundation for spatially informed depletion in MSR systems using a quasistatic approach to account for fuel circulation. This was performed using Griffin and the NEAMS coarse mesh thermal hydraulics code Pronghorn (Tano, 2023a). Preliminary work is underway to merge this new spatial depletion capability with the depletion-driven thermochemistry shown here. The end goal will be to fully couple Griffin, Thermochimica, and Pronghorn to leverage 3D temperatures/velocity fields to inform concentration gradients in the thermochemical equilibrium of MSR systems and more accurately determine the $f^{A}_{stream,Z}(t)$ term in Eq 7.

Additionally, redox corrosion kinetics plan to be incorporated in order to model short time frames where the molten salt is not in thermodynamic equilibrium represented by the $f^{A}_{chem,Z}(t)$ term in Eq 7. Uncertainty quantification and sensitivity studies can also be performed to see how uncertainties in nuclear data propagate changes in MSR thermochemistry throughout depletion. The comprehensive capability can also be applied towards performing material accountancy simulations that would be useful for safeguards and nonproliferation analyses.

The spatially informed depletion-driven thermochemistry model is expected be critical for understanding chemical species transport, deposition, dissolution, and corrosion during normal operation and accident scenarios. In this manner, multi-dimensional depletion-driven thermochemistry analyses of MSRs can be conducted to assess the space- and time-resolved chemistry of MSR systems.

5 Conclusion

A new multiphysics depletion-driven thermochemistry capability using NEAMS tools was developed and applied to analyze the role of depletion in altering the chemistry and multiphysics behavior of MSRs. The individual physics and coupled multiphysics methodology were introduced and discussed. While the capability in its current form is unable to provide absolute estimates for the redox potential in MSR systems (namely, due to database and code-coupling limitations), it can still generate informative results to model the chemical evaluation of both fluoride and chloride-based MSRs.

The phenomenon of depletion-driven thermochemistry is an essential aspect of MSR behavior and a critical starting point in analyzing these multiphysics systems. Specifically, this multiphysics phenomena dictates changes in corrosion, chemical speciation, and possible accident source terms. Consequentially, depletion-driven thermochemistry must be predicted for the reactor lifetime and subsequently measured and controlled by MSR instrumentation.

The result of this current work advances the state of the art of depletion-driven thermochemistry analysis by building a multiphysics framework using MOOSE-based NEAMS tools. The impact of this phenomena using the most up-to-date thermochemical data can be evaluated to a limited level of fidelity. This is expected to provide the foundation for more comprehensive models capturing more physics that impact species transport in MSRs.

More specifically, redox potential changes due to depletion can be modeled using this depletion-driven thermochemistry multiphysics capability over the reactor lifetime given the proper thermochemical data. This will allow upcoming MSR industry partners to accurately predict fuel salt behavior as depletion alters the chemistry of the system. Additionally, this work demonstrates how redox control mechanisms can be simulated over long periods of time. This is expected to help inform future instrumentation design for effective redox control of MSR systems. Lastly, this new capability can account for the change in element vapor pressures in the fuel salt as a function of burnup (and therefore redox potential). This is expected to be critical to performing source term calculations. Overall, this work is envisaged to lay the foundation for important design and licensing considerations of these multiphysics driven MSR systems.

Data availability statement

The original contributions presented in the study are included in the article/Supplementary material further inquiries can be directed to the corresponding author.

Author contributions

SW, MT, and AA-J contributed to conception and design of the study. OC contributed to developing new Griffin capabilities for multi-region microscopic depletion with nuclide feeds and SW contributed to testing and verifying these capabilities. SW, MT, and AA-J contributed to developing methodology approach for depletion-driven thermochemistry. SW and MT implemented the multiphysics coupling of Griffin and Thermochimica. MT enhanced coupling through Picard iterations. SW tested and verified capability of coupled multiphysics system. SW performed depletion-driven thermochemical analysis of MSR systems. SW wrote the first draft of manuscript. All authors contributed to the article and approved the submitted version.

Funding

This manuscript was authored at Idaho National Laboratory by Battelle Energy Alliance LLC under contract no. DE-AC07-05ID14517 with the U.S. Department of Energy (DOE). The funding agencies for this work are the DOE Office of Nuclear Energy programs: the Molten Salt Reactor campaign and the Nuclear Energy Advanced Modeling and Simulation (NEAMS) program.

Acknowledgments

This work was prepared for the U.S. DOE through a collaboration between the Molten Salt Reactor (MSR) campaign and the Nuclear Energy Advanced Modeling and Simulation (NEAMS) program. It made use of the resources of the High Performance Computing Center at Idaho National Laboratory, which is supported by the Office of Nuclear Energy of the U.S. Department of Energy and the Nuclear Science User Facilities under contract no. DE-AC07-05ID14517. The U.S. Government retains for itself, and others acting on its behalf, a paid-up nonexclusive, irrevocable worldwide license in said article to reproduce, prepare derivative works, distribute copies to the public, and perform publicly and display publicly, by or on behalf of the Government. The DOE will provide public access to these results of federally sponsored research in accordance with the DOE Public Access Plan: energy. gov/downloads/doe-public-access-plan. The authors would also like to thank Yaqi Wang, and Javier Ortensi of Idaho National Laboratory for their support with implementing modifications to the CRAM solver in Griffin. As well as Jacob Yingling for help with integrating the new version of MSTDB with Thermochimica, and for providing some helpful insight in understanding how Thermochimica processes results of the database. Lastly, the authors would like to thank Max Poschmann and Markus Piro from the University of Toronto, for their help with setting up the Thermochimica evaluations.

Conflict of interest

The authors declare that the research was conducted in the absence of any commercial or financial relationships that could be construed as a potential conflict of interest.

Publisher's note

All claims expressed in this article are solely those of the authors and do not necessarily represent those of their affiliated organizations, or those of the publisher, the editors and the reviewers. Any product that may be evaluated in this article, or claim that may be made by its manufacturer, is not guaranteed or endorsed by the publisher.

References

Abou-Jaoude, A., Harper, S., Giudicelli, G., Balestra, P., Schunert, S., Martin, N., et al. (2021). A workflow leveraging MOOSE transient multiphysics simulations to evaluate the impact of thermophysical property uncertainties on molten-salt reactors. *Ann. Nucl. Energy.* 163, 108546. doi:10.1016/j.anucene.2021.108546

Ard, J. C., Yingling, J. A., Johnson, K. E., Schorne-Pinto, J., Aziziha, M., Dixon, C. M., et al. (2022). Development of the molten salt thermal properties database – thermochemical (MSTDB–TC), example applications, and LiCl–RbCl and UF3–UF4 system assessments. *J. Nucl. Mat.* 563, 153631. doi:10.1016/j.jnucmat.2022.153631

Aufiero, M., Cammi, A., Fiorina, C., Leppänen, J., Luzzi, L., and Ricotti, M. (2013). An extended version of the SERPENT-2 code to investigate fuel burn-up and core material evolution of the Molten Salt Fast Reactor. *J. Nucl. Mat.* 441, 473–486. doi:10.1016/j.jnucmat.2013.06.026

Baes, C. F., Jr (1965). The chemistry and thermodynamics of molten salt reactor fluoride solutions. *J. Nucl. Mater.* 59, 149. United States. doi:10.2172/4576123

Baes, C. F., Jr (1974). The chemistry and thermodynamics of molten salt reactor fuels. *J. Nucl. Mat.* 51, 149–162. doi:10.1016/0022-3115(74)90124-X

Besmann, T. M., and Schorne-Pinto, J. (2021). Developing practical models of complex salts for molten salt reactors. *Thermo* 1, 168–178. doi:10.3390/thermo1020012

Chasanov, M. G. (1965). Fission-product effects in molten chloride fast-reactor fuels. *Nucl. Sci. Eng.* 23, 189–190. doi:10.13182/NSE65-A28145

Gougar, H. D., et al. (2015). *Assessment of the technical maturity of generation IV concepts for test or demonstration reactor applications, revision 2.* USDOE. *U. S.*

Graham, A. M., Taylor, Z., Collins, B. S., Salko, R. K., and Poschmann, M. (2021). Multiphysics coupling methods for molten salt reactor modeling and simulation in VERA. *Nucl. Sci. Eng.* 195, 1065–1086. doi:10.1080/00295639.2021.1901000

Guo, S., Shay, N., Wang, Y., Zhou, W., and Zhang, J. (2017). Measurement of europium (III)/europium (II) couple in fluoride molten salt for redox control in a molten salt reactor concept. *J. Nucl. Mat.* 496, 197–206. doi:10.1016/j.jnucmat.2017.09.027

Guo, S., Zhang, J., Wu, W., and Zhou, W. (2018). Corrosion in the molten fluoride and chloride salts and materials development for nuclear applications. *Prog. Mat. Sci.* 97, 448–487. doi:10.1016/j.pmatsci.2018.05.003

Haubenreich, P. N., and Engel, J. R. (1970). Experience with the molten-salt reactor experiment. *Nucl. Appl. Technol.* 8 (2), 118–136. doi:10.13182/NT8-2-118

Kelleher, B. C. (2013). *Purification and chemical control of molten Li_2BeF_4 salts for a fluoride salt cooled reactor.* [Madison (WI)]: University of Wisconsin-Madison. [dissertation thesis].

Kelleher, B., Dolan, K., Anderson, M., and Sridharan, K. (2016). Observed redox potential range of Li2BeF4 using a dynamic reference Electrode. *Nucl. Tech.* 195, 239–252. doi:10.13182/NT15-140

Lee, C., Viktor, C., and Paris, A. (2021). Griffin software development plan. United States. Technical Report ANL/NSE-21/23, INL/EXT-21-63185. Lemont, IL: Argonne National Laboratory, Idaho Falls, ID: Idaho National Laboratory. doi:10.2172/1845956

Martineau, R. C. (2021). The MOOSE multiphysics computational framework for nuclear power applications: A special issue of nuclear technology. *Nucl. Tech.* 207, 7. doi:10.1080/00295450.2021.1915487

McMuray, J. W., et al. (2018). *Multiphysics simulations for molten salt reactor evaluation: chemistry modeling and database development. United States*. Oak Ridge, TN: Oak Ridge National Laboratory. Technical report. doi:10.2171/1492183

McMurray, J. W., et al. (2021). Roadmap for thermal property measurements of Molten Salt Reactor systems. United States. Oak Ridge, TN: Oak Ridge National Laboratory. Technical Report ORNL/SPR-2020/1865. doi:10.2172/1778081

Mignacca, B., and Locatelli, G. (2020). Economics and finance of molten salt reactors. *Prog. Nucl. Energy.* 129, 103503. doi:10.1016/j.pnucene.2020.103503

Mourogov, A., and Bokov, P. M. (2006). Potentialities of the fast spectrum molten salt reactor concept: REBUS-3700. *Energy Conv. mgmt.* 47, 2761–2771. doi:10.1016/j.enconman.2006.02.013

Newton, M. L., Hamilton, D. E., and Simpson, M. F. (2020). Methods of redox control and measurement in molten NaCl-CaCl2-UCl3. *Trans. Elctro. Chem. Soc.* 98, 19–25. doi:10.1149/09810.0019ecst

Olander, D. (2002). Redox condition in molten fluoride salts: Definition and control. *J. Nucl. Mat.* 300, 270–272. doi:10.1016/S0022-3115(01)00742-5

Poschmann, M., Bajpai, P., Fitzpatrick, B. W., and Piro, M. H. (2021). Recent developments for molten salt systems in Thermochimica. *Calphad* 75, 102341. doi:10.1016/j.calphad.2021.102341

Poschmann, M., Piro, M. H., and Greenwood, M. S. (2022). Dynamic mass accountancy modeling of a molten salt reactor using equilibrium thermodynamics. *Nucl. Eng. Des.* 390, 111695. doi:10.1016/j.nucengdes.2022.111695

Shaffer, J. H. (1971). Preparation and handling of salt mixtures for the molten salt reactor experiment. United States. Oak Ridge, TN: Oak Ridge National Laboratory. Technical Report ORNL-4616. doi:10.2172/4074869

Shahbazi, S., et al. (2021). Thermochemical modeling in molten fluoride salts for radionuclide speciation, United States. doi:10.2172/1812872

Shahbazi, S., Romano, P., Fei, T., and Grabaskas, D. (2022b). Steady-state radiochemical transport model of the molten salt reactor experiment. *J. Radioanal. Nucl. Chem.* 331, 5247–5257. doi:10.1007/s10967-022-08535-3

Shahbazi, S. (2022a). *Survey of relevant data from the MSRP to guide development of MSR chemistry modeling benchmarks*. United States: Argonne National Lab. doi:10.2172/1962308

Tano, M. (2023a). Flow-informed corrosion in molten salts using the Poisson-Nernst-Planck model. *Proc. Nucl. React. Therm. Hydraul.* Accepted for Publication.

Tano, M. (2023b). Spatially resolved depletion studies of circulating fuel molten salt reactor systems. *Proc. Intl. Cong. Adv. Nucl. Pow. Plnts.* Paper #1339.

Thoma, R. E. (1971). Chemical aspects of MSRE operations. United States. Oak Ridge, TN: Oak Ridge National Laboratory. Technical Report ORNL-4658. doi:10.2172/4675946

Thomas, S., and Jerden, J. (2020). Mechanistic source term development for liquid fueled MSRs - model Development Update. United States. Technical Report ANL/CFCT-20/16. Lemont, IL: Argonne National Laboratory. doi:10.2172/1769029

Walker, S. A., et al. (2022). Implementation of isotopic removal capability in Griffin for multi-region MSR depletion analysis. *Trans. Am. Nucl. Soc.* 127 (1), 976–979.

Walker, S. A., et al. (2023). Leveraging coupled thermochemical depletion capabilities to evaluate off gas and source term characterization in molten salt reactor systems. *Proc. Intl. Cong. Adv. Nucl. Pow. Plnts.* Paper #1334.

Walker, S. A., and Ji, W. (2021b). Modeling corrosion product transport and reduction via beryllium addition in FLiBe molten salt. *Trans. Am. Nucl. Soc.* 125 (1), 135–138.

Walker, S. A., and Ji, W. (2021a). Species transport analysis of noble metal fission product transport, deposition, and extraction in the molten salt reactor experiment. *Ann. Nucl. Energy.* 158, 108250. doi:10.1016/j.anucene.2021.108250

Zhang, J., Forsberg, C. W., Simpson, M. F., Guo, S., Lam, S. T., Scarlat, R. O., et al. (2018). Redox potential control in molten salt systems for corrosion mitigation. *Corr. Sci.* 144, 44–53. doi:10.1016/j.corsci.2018.08.035

Nomenclature

R	Ideal Gas Constant [J/(mol - °K)]
T	Fuel-Salt or System Temperature [°K]
p_{F_2}	Partial Pressure of Fluorine Gas
$\Delta\bar{G}_{F_2}$	Fluorine Chemical Potential [J/mol]
F	Faraday's Constant [C/mol]
$n =$	Number of Electrons
E	Electrochemical Potential [V]
E^O	Standard Electrochemical Cell Potential [V]
Q	Reaction Quotient
$N_Z^A(t)$	Time Dependent Number Density of Nuclide with Mass Number A and Atomic Number Z [atoms/(b-cm)]
$N_{Z'}^{A'}(t)$	Time Dependent Number Density of Nuclide with Mass Number A′ and Atomic Number Z' [atoms/(b-cm)]
γ_Z^A	Fission Yield of Nuclide $N_Z^A(t)$ from Nuclide $N_{Z'}^{A'}(t)$
$\sigma_{f(Z',A'),g}(t)$	Time Dependent Groupwise Microscopic Fission Cross Section of Nuclide $N_{Z'}^{A'}(t)$ which Produces Nuclide $N_Z^A(t)$ [b]
$\phi_g(t)$	Time Dependent Groupwise Scalar Flux [neutrons/(cm^2 - s)]
$\sigma_{(Z',A')\rightarrow(Z,A),g}(t)$	Time Dependent Groupwise Microscopic Transmutation Cross Section of Nuclide $N_{Z'}^{A'}(t)$ which Produces Nuclide $N_Z^A(t)$ [b]
$r_{(Z',A')\rightarrow(Z,A)}$	Branching Ratio for Radioactive Decay of Nuclide $N_{Z'}^{A'}(t)$ which Produces Nuclide $N_Z^A(t)$
$\lambda_{Z'}^A$	Radioactive Decay Constant for Nuclide $N_{Z'}^A(t)$ [s^{-1} or Hz]
λ_Z^A	Radioactive Decay Constant for Nuclide $N_Z^A(t)$ [s^{-1} or Hz]
$\sigma_{a(Z,A),g}(t)$	Time Dependent Groupwise Absorption Cross Section for Nuclide $N_Z^A(t)$ [b]
$f_{chem,Z}^A(t)$	Time Dependent Chemical Reaction Source Term [atoms/(b - cm - s)]
$f_{stream,Z}^A(t)$	Time Dependent Mass Transfer Source Term [atoms/(b - cm - s)]
L	Mass Transfer Feed and Withdrawal Rate Coefficient [s^{-1} or Hz]
G	Gibbs Free Energy of the System [J/mol]
G^{ref}	Weighted Reference Gibbs Free Energy of System [J/mol]
$\Delta S =$	Change in Configurational Entropy of System [J/(mol - °K)]
G^{XS}	Excess Gibbs Energy or Gibbs Energy of Non-Ideal Mixing [J/mol]